



# Electrically induced bacterial membrane-potential dynamics correspond to cellular proliferation capacity

James P. Stratford<sup>a,b,1</sup>, Conor L. A. Edwards<sup>a,1</sup>, Manjari J. Ghanshyam<sup>a</sup>, Dmitry Malyshev<sup>a</sup>, Marco A. Delise<sup>a</sup>, Yoshikatsu Hayashi<sup>c</sup>, and Munehiro Asally<sup>a,b,d,2</sup>

<sup>a</sup>School of Life Sciences, University of Warwick, Coventry, West Midlands, CV4 7AL, United Kingdom; <sup>b</sup>Warwick Integrative Synthetic Biology Centre, University of Warwick, Coventry, West Midlands, CV4 7AL, United Kingdom; <sup>c</sup>Department of Biomedical Engineering, School of Biological Sciences, University of Reading, Reading, Berkshire, RG6 6AH, United Kingdom; and <sup>d</sup>Bio-Electrical Engineering Innovation Hub, University of Warwick, Coventry, West Midlands, CV4 7AL, United Kingdom

Edited by E. Peter Greenberg, University of Washington, Seattle, WA, and approved March 29, 2019 (received for review February 2, 2019)

**Membrane-potential dynamics mediate bacterial electrical signaling at both intra- and intercellular levels. Membrane potential is also central to cellular proliferation. It is unclear whether the cellular response to external electrical stimuli is influenced by the cellular proliferative capacity. A new strategy enabling electrical stimulation of bacteria with simultaneous monitoring of single-cell membrane-potential dynamics would allow bridging this knowledge gap and further extend electrophysiological studies into the field of microbiology. Here we report that an identical electrical stimulus can cause opposite polarization dynamics depending on cellular proliferation capacity. This was demonstrated using two model organisms, namely *Bacillus subtilis* and *Escherichia coli*, and by developing an apparatus enabling exogenous electrical stimulation and single-cell time-lapse microscopy. Using this bespoke apparatus, we show that a 2.5-second electrical stimulation causes hyperpolarization in unperturbed cells. Measurements of intracellular K<sup>+</sup> and the deletion of the K<sup>+</sup> channel suggested that the hyperpolarization response is caused by the K<sup>+</sup> efflux through the channel. When cells are preexposed to 400 ± 8 nm wavelength light, the same electrical stimulation depolarizes cells instead of causing hyperpolarization. A mathematical model extended from the FitzHugh–Nagumo neuron model suggested that the opposite response dynamics are due to the shift in resting membrane potential. As predicted by the model, electrical stimulation only induced depolarization when cells are treated with antibiotics, protonophore, or alcohol. Therefore, electrically induced membrane-potential dynamics offer a reliable approach for rapid detection of proliferative bacteria and determination of their sensitivity to antimicrobial agents at the single-cell level.**

bacterial electrophysiology | bioelectricity | cell biophysics | rapid bacterial detection | electrical signaling

Compared with animal bioelectrical signaling, bacterial electrical signaling is understudied and only recently were the excitation dynamics of membrane potential shown to mediate the intra- and intercellular signaling which regulates important physiological processes, namely mechanosensation, spore formation, and biofilm dynamics (1–4). In animal bioelectrical signaling, externally applied electrical stimuli and measurements of cellular electrical properties have been the principle methodology (5–8). This approach has led to many key discoveries regarding the roles of animal bioelectrical signaling [e.g., early tissue development (9, 10), regeneration (11), and carcinogenesis (12–14)] and has fostered the development of real-world applications such as for tissue engineering (15–17), wound healing (6, 18), and electroceuticals (19). Utilizing exogenous stimuli is an important step forward toward understanding bacterial electrical signaling and development of applications based on bacterial electrophysiology. In the past, applications of electric currents to bacteria were used for sanitization (20), electroporation (21), and most recently redox synthetic biology (22). However, due to the only recent discovery of bacterial membrane-potential excitation dynamics, use of external electrical signals in the context of bacterial electrophysiology has been left largely unexplored.

An external electrical stimulus alters cellular membrane potential according to the Schwan equation:  $\Delta\psi_{max} = \Delta\psi_{max} = 1.5aE(1 + (2\pi f\tau)^2)^{-\frac{1}{2}}$ , where  $\Delta\psi_{max}$  is the induced membrane potential,  $a$  is the cell radius,  $E$  is the applied field strength,  $f$  is the AC field frequency, and  $\tau$  is the relaxation time of the membrane (23). This equation, derived from the electromagnetic theory (24), expresses that the maximum change in the membrane potential of a cell caused by an electrical stimulus is proportional to the applied field strength. Theoretically, when an electrical stimulus is applied to proliferative bacterial cells, it should lead to opening of voltage-gated K<sup>+</sup> channels (Kv) and consequent hyperpolarization due to K<sup>+</sup> efflux. Substituting the typical values of bacterial resting potential [−140 ~ −75 mV (25, 26)] and threshold potential for Kv [−50 mV (27)] to the equation, one can expect that the depolarization by an electrical stimulus with the field strength of +35 ~ 120 mV/μm should open voltage-gated K<sup>+</sup> channels on bacteria.

In addition to its role in bioelectrical signaling, membrane potential is central to cellular proliferation; it provides the essential driving force for ATP synthesis (28) and is crucial for cell division (29). A quantitative estimation based on the measured

## Significance

**Transmembrane voltage in bacteria plays a central role both in electrical signaling and cell proliferation. However, whether proliferation state influences the response to electrical signals was unknown. Combining fluorescence time-lapse microscopy with a bespoke device and mathematical modeling, we show that proliferative and inhibited cells respond in opposite directions to an identical electrical signal. The response differentiation can be seen within a minute after stimulation. Therefore, our findings offer an approach for rapid detection of proliferative bacteria at the single-cell level.**

Author contributions: J.P.S. and M.A. designed research; J.P.S., C.L.A.E., M.J.G., D.M., M.A.D., Y.H., and M.A. performed research; J.P.S., C.L.A.E., M.A.D., Y.H., and M.A. contributed new reagents/analytic tools; C.L.A.E., M.J.G., D.M., and M.A. analyzed data; and M.A. wrote the paper.

Conflict of interest statement: Based on the findings of this work, a UK patent application for the approach of rapidly detecting proliferative bacteria using electricity has been filed and a spin-out company (Cytecom Ltd.) was founded with the support from the University of Warwick. The spin-out company and the corresponding author (M.A.) were awarded the funding for the commercialization of the technology from United Kingdom Research and Innovation (UKRI), the UK national funding agency. The authors clarify that the scientific conclusions that are presented in this study are not influenced by the activity of the spin-out company.

This article is a PNAS Direct Submission.

This open access article is distributed under [Creative Commons Attribution License 4.0 \(CC BY\)](https://creativecommons.org/licenses/by/4.0/).

<sup>1</sup>J.P.S. and C.L.A.E. contributed equally to this work.

<sup>2</sup>To whom correspondence should be addressed. Email: [m.asally@warwick.ac.uk](mailto:m.asally@warwick.ac.uk).

This article contains supporting information online at [www.pnas.org/lookup/suppl/doi:10.1073/pnas.1901788116/-DCSupplemental](https://www.pnas.org/lookup/suppl/doi:10.1073/pnas.1901788116/-DCSupplemental).

Published online April 18, 2019.





response in the timescale of  $\sim 5$  s, the hyperpolarization response on the timescale of  $\sim 30$  s is greatly attenuated (Fig. 1 *D* and *E* and *SI Appendix*, Fig. S4*B*). For a further test, we measured the intracellular  $K^+$  levels using Asante Potassium Green-2 AM (APG-2 AM) (2), and found that the intracellular  $K^+$  decreases upon stimulation (*SI Appendix*, Fig. S8). These results suggest that  $K^+$  efflux through the YugO channel is responsible for the hyperpolarization following an electrical stimulation. It also suggests that there may be other voltage-gated channels with faster timescales of activation and inactivation ( $\sim 5$  s). It is worth noting that bacteria have several voltage-gated ion channels (4, 41, 42). This is an interesting observation in conjunction with the fact that different neural ion channels have their unique timescales of activation and inactivation which contribute to information processing (27). We also conducted the same experiment with *E. coli* and confirmed that *E. coli* cells also exhibit hyperpolarization in response to an external electrical stimulus (*SI Appendix*, Fig. S9). Together, these results demonstrate with single-cell resolution that a pulsed electrical stimulus can induce a hyperpolarization response in bacterial cells.

**Exposure to UV-Violet Light Abolishes Hyperpolarization Response to an Electrical Stimulus.** Having tested our apparatus, we examined the impact of proliferative capacity on signal response by using inhibited cells. To inhibit the proliferative capacity of cells, we chose UV-Violet light (400 nm) because it is one of the most commonly used sanitization methods, which has been shown to be effective with both Gram-positive and Gram-negative bacteria (43, 44). Importantly, application of UV-V light allows spatially precise inhibition, creating both irradiated and unirradiated regions within the same field of view. This is critical because it ensures that an identical electrical stimulation is applied to both proliferative and inhibited cells. We irradiated *B. subtilis* cells in a defined region by UV-V light for 30 s (Fig. 2*A*). The growth suppression of the irradiated cells was confirmed by the single-cell analysis of phase-contrast time-lapse microscopy before being stimulated with an electrical pulse (*SI Appendix*, Fig. S10). Upon an electrical stimulation, the irradiated cells exhibit depolarization, while cells in untreated regions become hyperpolarized, despite the fact that both received an identical electrical stimulus (Fig. 2*B* and *C*). This experiment demonstrates that an electrical stimulus can result in cellular response in apparent opposite directions depending on whether cells are exposed to UV-V or not. Strikingly, analysis of the fluorescence dynamics after electrical stimulation showed a clear bimodal distribution correlating with the irradiation (*SI Appendix*, Fig. S11*A* and *B*). To examine whether this is unique to *B. subtilis*, we conducted the same experiment with *E. coli* cells. The result with *E. coli* also revealed distinct responses depending on whether cells were treated by UV-V or not (*SI Appendix*, Fig. S11*C*). These results suggest that proliferative and growth-inhibited cells respond differently to an identical electrical stimulus and that this difference in response dynamics is common to these two phylogenetically distant model organisms.

**A Mathematical Model Suggests That the Response Differentiation Is Due to the Shift in Resting Membrane Potential.** To gain conceptual understanding of the observed distinct responses to an identical electrical stimulus, we used a mathematical framework based on the FitzHugh-Nagumo (FHN) neuron model. The FHN neuron model, originally published over half a century ago (45), is one of the most paradigmatic models in neuroscience due to its mathematical simplicity and richness for capturing complex behaviors (46). We extended the FHN neuron model to bacterial electrophysiology while retaining its mathematical simplicity (*SI Appendix* for details). Briefly, in our FHN bacteria model, we considered two parameters representing the resting-state membrane potential and  $K^+$  transmembrane gradient. Numerical simulations of the model showed that an external electrical

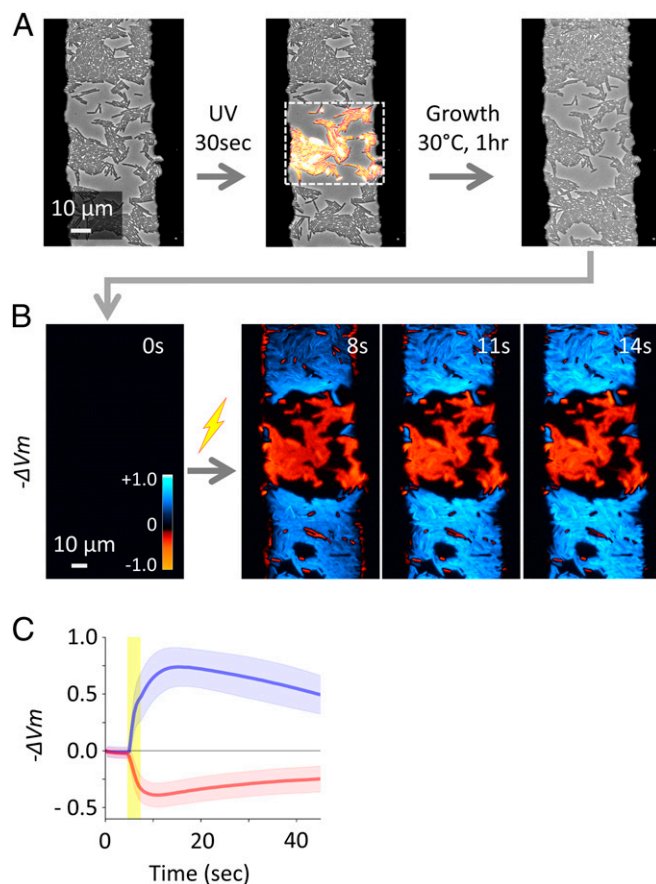


**Fig. 2.** UV-V irradiation makes *B. subtilis* cells respond to an electrical stimulus in the opposite direction. (A) Phase-contrast microscopy image shows WT *B. subtilis* cells within the electrode gap. A rectangular region indicated by the dashed line within the field of view was irradiated by UV-V light. Growth was suppressed in the UV-irradiated region, while cells outside of the UV-irradiation region replicated. (B) The region shown in A was treated with an electrical stimulus.  $-\Delta V_m$  was calculated from ThT fluorescence [ $\log(F_{ThT}/F_{ThT,R})$ ] and shown with the colormap in the panel. To an identical electrical stimulus, unperturbed cells hyperpolarized (blue) and UV-V-irradiated cells depolarized (red). (C) Mean (thick lines) and SD (shaded color) of  $-\Delta V_m$  for cells in unperturbed (blue) and UV-V-irradiated (red) regions.

stimulus causes hyperpolarization in proliferative cells, while the same stimulus produces a relaxation response from depolarization in inhibited cells (Fig. 3*A* and *SI Appendix*, Fig. S12). This is because the direction of  $K^+$  flux (influx or efflux) differs depending on the resting-state membrane potential and transmembrane concentration gradient of  $K^+$  (Fig. 3*B*). According to our simulations, opening of  $K^+$  channels in proliferative cells results in  $K^+$  efflux following the concentration gradient, thus causing hyperpolarization. However, the same opening of  $K^+$  channels only leads to the relaxation from depolarization due to weaker transmembrane  $K^+$  gradient. This mechanistic insight from the simulations predicts that the shift in resting-state membrane potential is sufficient to alter the response dynamics to an electrical stimulus. This means that different classes of growth-inhibition treatments should also make cells respond by depolarization.

To examine this prediction from the model, we conducted the electrical stimulation experiment with the cells exposed to different classes of common growth-inhibition treatments; namely, an antibiotic vancomycin, a protonophore carbonyl cyanide *m*-chlorophenyl hydrazone (CCCP), and a common antimicrobial agent ethanol. As predicted by the model, vancomycin-treated

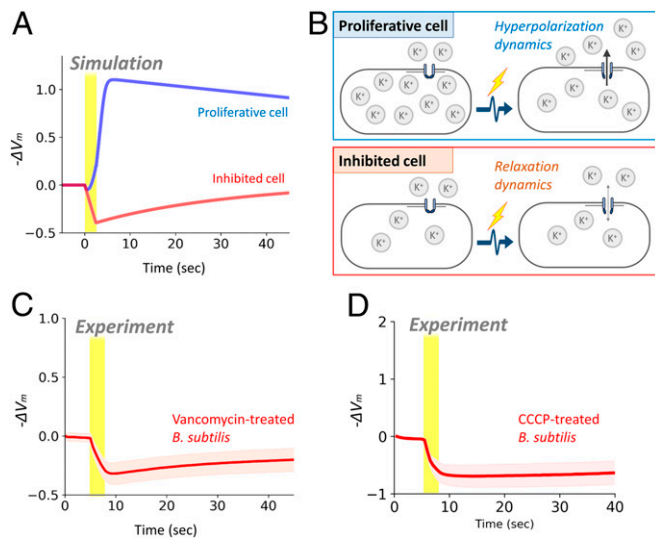


**Fig. 3.** Shift in resting-state membrane potential is sufficient to describe the distinct responses between proliferative and inhibited cells. (A) Numerical simulation of the FHN bacteria model, corresponding to Fig. 2C. Despite being stimulated by an identical electrical stimulus, proliferative cells (blue) hyperpolarize and inhibited cells (red) depolarize. See *SI Appendix* for model details. (B) Illustration of the biological mechanism of the response differentiation between proliferative and inhibited cells. (C and D) Time trace of membrane potential change ( $-\Delta V_m$ ) with *B. subtilis* cells exposed to (C) vancomycin or (D) CCCP. Shading shows SD.

cells exhibited a clear depolarization in response to an exogenous electrical stimulus (Fig. 3C), as opposed to the hyperpolarization response seen in unperturbed cells (Fig. 1C). Experimental tests with the cells treated with ethanol or CCCP also showed depolarization response (Fig. 3D and *SI Appendix*, Fig. S13). These results strongly support the conclusion drawn from the FHN model that general stress treatments alter the cellular response to an electrical stimulus. Conversely, this finding suggests that the proliferative and inhibited cells can be distinguished based on their response to an exogenous electrical stimulus.

**Selective Antibiotics Enable Classification of Coliforms in a Mixed Culture.** The above observations and understanding raised the possibility of using the electrically induced membrane-potential dynamics for rapid detection of proliferative cells in a mixed-species culture. Such application would be significant to industries and medical sectors as it can offer rapid single-cell level detection of proliferative cells of biological samples. For proof of concept, we explored this possibility using a coculture of *E. coli* (gram-negative) and *B. subtilis* (gram-positive). Our hypothesis was that the above approach of measuring electrically induced membrane-potential dynamics combined with exposure to vancomycin allows for the rapid differentiation of *E. coli* and *B. subtilis*. This is based on the fact that vancomycin inhibits the cell-wall synthesis of gram-positives but is largely inactive to gram-negatives due to their outer membrane barrier (47).

To test this hypothesis, we cocultured fluorescently labeled strains of *E. coli* and *B. subtilis* expressing mCherry and YFP under IPTG-inducible promoters for *E. coli* and *B. subtilis*, respectively. Multichannel fluorescence imaging exhibited distinct signals for *E. coli* and *B. subtilis* (Fig. 4A). The fluorescence of ThT showed lower intensity with *E. coli* compared with *B. subtilis* (Fig. 4B). Although the exact reason for this is unclear it may suggest that there is a difference in stability or fluorescence yield of ThT between these two species. This difference in intensity highlights an advantage of our approach focusing on the response dynamics rather than being reliant on the initial affinity of

the cells for the dye. After an hour-long exposure to vancomycin, the coculture was treated with an external electrical stimulus. The result revealed distinct patterns of membrane-potential dynamics for *E. coli* and *B. subtilis* cells treated with vancomycin. Specifically, the electrical stimulation causes *E. coli* to become hyperpolarized, while depolarizing vancomycin-treated *B. subtilis* (Fig. 4C and D and *SI Appendix*, Fig. S14). Similar patterns were observed with monocultures of *E. coli* or *B. subtilis* (*SI Appendix*, Fig. S15). We also confirmed that vancomycin is active on *B. subtilis*, but not on *E. coli* (*SI Appendix*, Fig. S16). The histogram of individual-cell response revealed distinct distributions between *E. coli* and *B. subtilis* (Fig. 4E). These results thus demonstrate that our approach can be combined with selective culture methods that are commonly used for species differentiation.

## Discussion

In this study, we developed and demonstrated an experimental tool for studying the input–output relation of bacterial electrical signaling. Using this tool combined with time-lapse microscopy, we showed that proliferative and inhibited cells respond to an electrical stimulation in apparent opposite directions. A mathematical model suggested that the apparent opposite responses can arise from diverse antibacterial stresses. We experimentally confirmed this using UV-V light, antibiotics, ethanol, and CCCP. The distinct response dynamics between proliferative and inhibited cells offer a rapid single-cell detection of proliferative cells, which can be combined with differentiation techniques using selective growth media.

Bacterial electrical signaling mediated by membrane-potential dynamics regulates various physiological processes, such as metabolic coordination in biofilms and mechanosensation (4, 48). However, it remains unclear how cells decode various information from the received electrical signal. We demonstrated that proliferation capacity adds to the complexity of bacterial electrical signaling, which presents a clue for elucidating the signal-decoding mechanism. Recent study showed that only a subpopulation of cells contributes to the biofilm electrical signaling, which optimizes the cost–benefit tradeoff of signal transmission (49). Cell-to-cell heterogeneity in electrical signaling is also observed in mechanosensation (4), sporulation (3), and antibiotics stress response (50). These heterogeneities are important for understanding how cells decode electrical signal

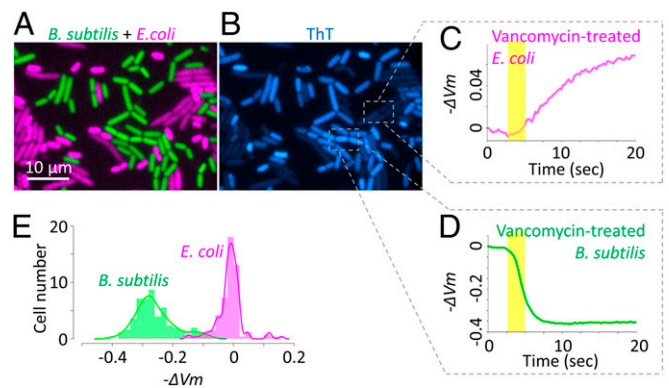


**Fig. 4.** When treated with vancomycin, *B. subtilis* and *E. coli* cells can be differentiated based on their response to an electrical stimulus. (A) Microscopy image showing the coculture of fluorescently labeled *E. coli* (magenta) and *B. subtilis* (green) cells treated with vancomycin. (B) ThT fluorescence image at the corresponding region. (C and D) Time trace of  $-\Delta V_m$ , calculated from ThT fluorescence intensity, of the regions defined in B. (E) Histogram of  $-\Delta V_m$  at 10 s after electrical stimulation of *B. subtilis* and *E. coli* shows clear differentiation of peaks with the presence of vancomycin.



inputs. However, the mechanisms by which these heterogeneities emerge remain unclear. Our finding raises a possibility that the variations in proliferative capacity may underpin the signaling heterogeneities since the bidirectional interaction between metabolisms and electrical signaling could in theory induce multi-stability in the system. We expect that future mathematical and computational studies, combined with single-cell analyses, will investigate the input–output relation and information processing of bacterial electrical signaling.

We showed, through the combination of simulations and experiments, that the distinct response dynamics between proliferative and inhibited cells can be described by the shift in resting membrane potential. Since the maintenance of membrane potential accounts for a major fraction of cellular energy consumption (30), it seems plausible that different types of metabolic and environmental stress would all ultimately lead to imbalance in transmembrane ion gradient at resting state. For instance, the Ktr potassium uptake system in *B. subtilis* and the Kdp potassium uptake system in *E. coli* are both ATP driven (51, 52). This means that maintaining the resting-state membrane potential requires constant consumption of ATP to keep the intracellular  $K^+$  level up to two orders of magnitude higher than the outside. When an electrical stimulus opens voltage-gated  $K^+$  channels, the flux of  $K^+$  through the channel follows the electrochemical gradient of  $K^+$ , which indicates that hyperpolarization due to  $K^+$  efflux occurs only when intracellular  $K^+$  concentration is significantly greater than the extracellular level. This effect was accounted for by the parameter  $k_K$  in our FHN bacteria model (*SI Appendix*). Using the tool, we will be able to carry out future studies to quantitatively analyze the dynamics of other electrophysiologically important ions, such as  $Ca^{2+}$  and  $Cl^-$  and determine their contributions to the membrane-potential dynamics in bacteria. Biological and biophysical characterization of the dynamics of transmembrane gradients of different ions and their corresponding channels will form the fundamental basis to our understanding of bacterial electrical signaling. Another important area of research is to identify the molecular mechanism by which electrical stimuli open the YugO potassium channel.

We hope that the experimental setup developed and demonstrated in this work will encourage more microbiologists to consider bacterial electrophysiology for gaining new insights into their physiological processes of interest. Although it is known that membrane potential is closely associated with important microbiological processes, including persister formation and antibiotics resistance (53–56), biological and mechanistic insights into such relation are largely limited. This is partly because of the shortage of appropriate experimental tools for molecular microbiology investigations. Recent discoveries of various signaling roles for bacterial membrane potential and ion flux (1, 2, 50, 57) suggest that bacterial electrical signaling may play roles in many more physiological processes than previously realized. The uses of exogenous electrical stimuli should unlock opportunities to gain new biological insights regarding signaling roles of membrane-potential dynamics. In parallel, it will also facilitate the development into new synthetic-biology technologies for electrical control and bioelectrical engineering of bacterial functions.

Finally, our findings offer an approach for rapid detection of proliferative bacteria without the need for observing actual proliferation or the time-consuming calibrations for bacterial species. The growing demand for fast identification of live bacterial cells has been driving the development of novel technologies for rapid bacterial detection (58). Our approach could detect proliferative cells within a minute after an electrical stimulation, as opposed to the typical duration of 12–48 h required by conventional culture-based detection methods (58). This attractive feature could accelerate the examination of antimicrobial agents and diagnosis in the medical sector and enable efficient quality control in the water, pharmaceutical, food, and

beverage industries. The capability to differentiate UV-damaged cells from healthy cells is also unique. In further studies, we will examine if this approach enables the detection of medically and industrially relevant bacterial species for timely diagnosis. If applied widely, this approach of using membrane-potential dynamics and exogenous electrical stimuli could bring great societal benefits by accelerating the detection of proliferative bacteria and determination of their sensitivity to antimicrobial agents.

## Materials and Methods

**Strains and Growth Conditions.** *E. coli* and *B. subtilis* cells were routinely grown in lysogeny broth (LB) or on an LB agar [1.5% (wt/vol)] plate. The reporter and mutant strains used in this study are listed in *SI Appendix, Table S1*. For electrical stimulation experiments, a colony from an LB agar plate was inoculated into liquid LB and subsequently incubated at 30 °C with aeration (200 rpm; model 311DS, Labnet) to  $OD_{600} \sim 1.5$ . Cells were then resuspended in minimal salts glutamate glycerol (MSgg) media (59): 5 mM potassium phosphate (pH 7.0), 10 mM Mops (pH 7.0), 2 mM  $MgCl_2$ , 700  $\mu M$   $CaCl_2$ , 50  $\mu M$   $MnCl_2$ , 100  $\mu M$   $FeCl_3$ , 1  $\mu M$   $ZnCl_2$ , 2  $\mu M$  thiamine-HCl, 0.5% (vol/vol) glycerol, and 0.5% (wt/vol) monosodium glutamate. Note that the Mops concentration is reduced by 10-fold from the original receipt of MSgg to suppress electrolysis of the media. After a 1-h incubation in liquid MSgg, cells were inoculated onto MSgg low-melting point (LMP) agarose pads containing 10  $\mu M$  ThT (Sigma-Aldrich). With experiments focusing on mixed culture, 5  $\mu g/mL$  vancomycin hydrochloride, 1 mM  $NH_4Cl$ , and 0.25% (wt/vol) glucose were supplemented to the MSgg LMP agarose pads. Pads were prepared as described previously (60). Briefly, LMP agarose (Formedium, bacteriological granulated agar) was dissolved in MSgg and left to solidify between two 22 mm  $\times$  22 mm cover glasses (Fisher Scientific) for 10 min at room temperature. When stated, final concentration of 1% (vol/vol) ethanol or 100  $\mu M$  CCCP was supplemented to MSgg liquid and MSgg agarose pads. For the measurements of intracellular  $K^+$ , APG-2 (Abcam PLC), instead of ThT, was supplemented to MSgg agarose pads at the final concentration of 2  $\mu M$ . The solidified agar was cut into  $\sim 5$  mm  $\times$  5 mm pads. A total of 2  $\mu L$  of bacterial liquid LB culture ( $OD_{600} \sim 1.5$ ) was inoculated onto each pad. Pads were then placed on the gold-coated glass-bottom dish for microscopy.

For the construction of *E. coli* K12 pGEX6P1-mCherry strain, pGEX-6P1 plasmid (GE Healthcare) was digested with EcoRI and NotI restriction enzymes (New England Biolabs). The mCherry gene was amplified by PCR using PrimeSTAR Max DNA Polymerase (Takara Bio) using the primers AP609 (5'-CCCCTGGGATCCCCGGAATTCATGTGAGCAAGGCGAG-3') and AP610 (5'-AGTCACGATGCGCGCTCGAGTTTAGCACTTGACAGTTCTGCCATG-3'). The PCR product was assembled together with the digested pGEX-6p1 by the Gibson Assembly using Gibson Assembly Master Mix kit (New England Biolabs) and transformed into competent *E. coli* K12 cells. The competent cells were prepared using Mix&Go Competent Cells kit (Zymo Research). The sequence of the assembled plasmids was confirmed by Sanger sequencing (Source BioScience) and aligned using Benchling (<https://benchling.com/>).

**Electrical Stimulation.** Application of electrical stimulation was accompanied with time-lapse imaging with 2 frames per second (fps) for 1 min. An alternating current (AC) signal [0.1 kHz; 3 V peak-to-peak ( $-1.5 \sim +1.5$  V)] was generated using an arbitrary function generator (Tektronics) and connected to a series of relays, each corresponding to an electrode on the gold-coated dish (*SI Appendix, Fig. S2*). The camera trigger was connected to Arduino UNO R3 in the relay circuit to control the timing of electrical stimulation; upon counting 10 camera exposures, the relay to the electrode being imaged opened for 2.5 s, applying electrical stimulation to the electrode while simultaneously imaging.

**Time-Lapse Microscopy.** The membrane-potential dynamics and growth of individual cells were recorded using an inverted epifluorescence microscope, DMi8 (Leica Microsystems), operated by MetaMorph (Molecular Devices). The microscope is equipped with an incubation chamber (i8 Incubator; Pecon) which maintained the temperature at 30 °C throughout the experiments. Before microscopy experiments, the chamber was set to 30 °C for at least 3 h, and samples were placed in the chamber for 1 h. For all observations, a 100 $\times$  objective lens (N.A. = 1.3, HCX PL FLUOTAR; Leica) was used and images were taken with scientific CMOS camera ORCA-Flash 4.0 v2 (Hamamatsu Photonics). Cell growth was monitored using phase contrast (exposure time: 100 ms). ThT fluorescence was detected using a single-band filter set consisting of excitation filter (Ex) 438/24 nm, emission filter (Em) 483/32 nm, and dichroic mirror 458 nm (Semrock), with exposure time of 150 ms. For the mixed culture experiment, YFP was detected using a filter set consisting of Ex 509/22, Em 544/24, and dichroic mirror 526 (Semrock). mCherry was detected

using a filter set consisting of Ex 554/23, Em 609/54, and dichroic mirror 573 (Semrock). The exposure time for the imaging of both YFP and mCherry was 300 ms.

For irradiation to UV violet light, cells were irradiated by UV-Violet light for 30 s using the inverted microscope DMI8 (Leica Microsystems) and the LED light source, SOLA SM II Light Engine (Lumencor), with an excitation filter 400/16. Field diaphragm of the microscope was used to irradiate only a specific region of the field of view. Before electrical stimulation, a 1-h growth period was allowed during which cells were observed using phase-contrast microscopy to ascertain the effects of UV-V light. For ethanol experiments, MSgg containing 1% (vol/vol) ethanol was used instead of MSgg.

- Lee DD, Prindle A, Liu J, Sül GM (2017) SnapShot: Electrochemical communication in biofilms. *Cell* 170:214–214.e1.
- Prindle A, et al. (2015) Ion channels enable electrical communication in bacterial communities. *Nature* 527:59–63.
- Sirec T, Buffard P, Garcia-Ojalvo J, Asally M (2018) Electrical-charge accumulation enables integrative quality control during *B. subtilis* sporulation. bioRxiv:10.1101/349654. Preprint, posted June 20, 2018.
- Bruni GN, Weekley RA, Dodd BJT, Kralj JM (2017) Voltage-gated calcium flux mediates *Escherichia coli* mechanosensation. *Proc Natl Acad Sci USA* 114:9445–9450.
- Piccolino M (1997) Luigi Galvani and animal electricity: Two centuries after the foundation of electrophysiology. *Trends Neurosci* 20:443–448.
- McCaig CD, Rajniecek AM, Song B, Zhao M (2005) Controlling cell behavior electrically: Current views and future potential. *Physiol Rev* 85:943–978.
- Chang F, Minc N (2014) Electrochemical control of cell and tissue polarity. *Annu Rev Cell Dev Biol* 30:317–336.
- Robinson KR (1985) The responses of cells to electrical fields: A review. *J Cell Biol* 101:2023–2027.
- Adams DS, Levin M (2013) Endogenous voltage gradients as mediators of cell-cell communication: Strategies for investigating bioelectrical signals during pattern formation. *Cell Tissue Res* 352:95–122.
- Levin M (2014) Molecular bioelectricity: How endogenous voltage potentials control cell behavior and instruct pattern regulation in vivo. *Mol Biol Cell* 25:3835–3850.
- Levin M (2007) Large-scale biophysics: Ion flows and regeneration. *Trends Cell Biol* 17:261–270.
- Lobikin M, Chernet B, Lobo D, Levin M (2012) Resting potential, oncogene-induced tumorigenesis, and metastasis: The bioelectric basis of cancer in vivo. *Phys Biol* 9:065002.
- Yang M, Brackenbury WJ (2013) Membrane potential and cancer progression. *Front Physiol* 4:185.
- Pardo LA, Stühmer W (2014) The roles of K(+) channels in cancer. *Nat Rev Cancer* 14:39–48.
- Markx GH (2008) The use of electric fields in tissue engineering: A review. *Organogenesis* 4:11–17.
- Tandon N, et al. (2009) Electrical stimulation systems for cardiac tissue engineering. *Nat Protoc* 4:155–173.
- Levin M, Pezzulo G, Finkelstein JM (2017) Endogenous bioelectric signaling networks: Exploiting voltage gradients for control of growth and form. *Annu Rev Biomed Eng* 19:353–387.
- Hunckler J, de Mel A (2017) A current affair: Electrotherapy in wound healing. *J Multidiscip Healthc* 10:179–194.
- Famm K, Litt B, Tracey KJ, Boyden ES, Slaoui M (2013) Drug discovery: A jump-start for electroceuticals. *Nature* 496:159–161.
- Hfilshager H, Potel J, Niemann E-G (1981) Killing of bacteria with electric pulses of high field strength. *Radiat Environ Biophys* 20:53–65.
- Chassy BM, Mercenier A, Flickinger J (1988) Transformation of bacteria by electroporation. *Trends Biotechnol* 6:303–309.
- Schloss AC, et al. (2016) Fabrication of modularly functionalizable microcapsules using protein-based technologies. *ACS Biomater Sci Eng* 2:1856–1861.
- Marszalek P, Liu DS, Tsong TY (1990) Schwan equation and transmembrane potential induced by alternating electric field. *Biophys J* 58:1053–1058.
- Kotnik T, Miklavcic D (2000) Analytical description of transmembrane voltage induced by electric fields on spheroidal cells. *Biophys J* 79:670–679.
- Felle H, Porter JS, Slayman CL, Kaback HR (1980) Quantitative measurements of membrane potential in *Escherichia coli*. *Biochemistry* 19:3585–3590.
- Ramos S, Schuldiner S, Kaback HR (1976) The electrochemical gradient of protons and its relationship to active transport in *Escherichia coli* membrane vesicles. *Proc Natl Acad Sci USA* 73:1892–1896.
- Zheng J, Trudeau MC (2015) *Handbook of Ion Channels*, eds Zheng J, Trudeau M (CRC Press, Boca Raton, FL).
- Kaim G, Dimroth P (1999) ATP synthesis by F-type ATP synthase is obligatorily dependent on the transmembrane voltage. *EMBO J* 18:4118–4127.
- Strahl H, Hamoen LW (2010) Membrane potential is important for bacterial cell division. *Proc Natl Acad Sci USA* 107:12281–12286.
- Milo R, Phillips R (2015) *Cell Biology by the Numbers* (Garland Science, New York).
- Mason DJ, López-Amorós R, Allman R, Stark JM, Lloyd D (1995) The ability of membrane potential dyes and calcafluor white to distinguish between viable and non-viable bacteria. *J Appl Bacteriol* 78:309–315.
- Breeuwer P, Abee T (2000) Assessment of viability of microorganisms employing fluorescence techniques. *Int J Food Microbiol* 55:193–200.
- Cléach J, et al. (2018) Use of ratiometric probes with a spectrofluorometer for bacterial viability measurement. *J Microbiol Biotechnol* 28:1782–1790.
- Kralj JM, Hochbaum DR, Douglass AD, Cohen AE (2011) Electrical spiking in *Escherichia coli* probed with a fluorescent voltage-indicating protein. *Science* 333:345–348.
- Alteri CJ, Lindner JR, Reiss DJ, Smith SN, Mobley HLT (2011) The broadly conserved regulator PhoP links pathogen virulence and membrane potential in *Escherichia coli*. *Mol Microbiol* 82:145–163.
- Sträuber H, Müller S (2010) Viability states of bacteria—Specific mechanisms of selected probes. *Cytometry A* 77:623–634.
- Zhang Z, Milias-Argetis A, Heinemann M (2018) Dynamic single-cell NAD(P)H measurement reveals oscillatory metabolism throughout the *E. coli* cell division cycle. *Sci Rep* 8:2162.
- Shinar G, Milo R, Martinez MR, Alon U (2007) Input output robustness in simple bacterial signaling systems. *Proc Natl Acad Sci USA* 104:19931–19935.
- Kubitschek HE (1969) Growth during the bacterial cell cycle: Analysis of cell size distribution. *Biophys J* 9:792–809.
- Jayaram DT, Luo Q, Thourson SB, Finlay AH, Payne CK (2017) Controlling the resting membrane potential of cells with conducting polymer microwires. *Small* 13:1700789.
- Ren D, et al. (2001) A prokaryotic voltage-gated sodium channel. *Science* 294:2372–2375.
- Payandeh J, Minor DL, Jr (2015) Bacterial voltage-gated sodium channels (BacNa(V)s) from the soil, sea, and salt lakes enlighten molecular mechanisms of electrical signaling and pharmacology in the brain and heart. *J Mol Biol* 427:3–30.
- Murdoch LE, Maclean M, Endarko E, MacGregor SJ, Anderson JG (2012) Bactericidal effects of 405 nm light exposure demonstrated by inactivation of *Escherichia*, *Salmonella*, *Shigella*, *Listeria*, and *Mycobacterium* species in liquid suspensions and on exposed surfaces. *ScientificWorldJournal* 2012:137805.
- Maclean M, Murdoch LE, MacGregor SJ, Anderson JG (2013) Sporocidal effects of high-intensity 405 nm visible light on endospore-forming bacteria. *Photochem Photobiol* 89:120–126.
- Fitzhugh R (1961) Impulses and physiological states in theoretical models of nerve membrane. *Biophys J* 1:445–466.
- Mallot HA (2013) *Computational Neuroscience* (Springer International Publishing, Heidelberg).
- Nikaïdo H (1989) Outer membrane barrier as a mechanism of antimicrobial resistance. *Antimicrob Agents Chemother* 33:1831–1836.
- Liu J, et al. (2015) Metabolic co-dependence gives rise to collective oscillations within biofilms. *Nature* 523:550–554.
- Larkin JW, et al. (2018) Signal percolation within a bacterial community. *Cell Syst* 7:137–145.e3.
- Lee DD, et al. (February 28, 2019) Magnesium flux modulates ribosomes to increase bacterial survival. *Cell*, 10.1016/j.cell.2019.01.042.
- Vieira-Pires RS, Szollosi A, Morais-Cabral JH (2013) The structure of the KtrAB potassium transporter. *Nature* 496:323–328.
- Haupt M, Bramkamp M, Coles M, Kessler H, Altendorf K (2005) Prokaryotic Kdp-ATPase: Recent insights into the structure and function of KdpB. *J Mol Microbiol Biotechnol* 10:120–131.
- Verstraeten N, et al. (2015) O<sub>2</sub> and membrane depolarization are part of a microbial bet-hedging strategy that leads to antibiotic tolerance. *Mol Cell* 59:9–21.
- Damper PD, Epstein W (1981) Role of the membrane potential in bacterial resistance to aminoglycoside antibiotics. *Antimicrob Agents Chemother* 20:803–808.
- Allison KR, Brynildsen MP, Collins JJ (2011) Heterogeneous bacterial persisters and engineering approaches to eliminate them. *Curr Opin Microbiol* 14:593–598.
- Allison KR, Brynildsen MP, Collins JJ (2011) Metabolite-enabled eradication of bacterial persisters by aminoglycosides. *Nature* 473:216–220.
- Humphries J, et al. (2017) Species-independent attraction to biofilms through electrical signaling. *Cell* 168:200–209.e12.
- Ahmed A, Rushworth JV, Hirst NA, Millner PA (2014) Biosensors for whole-cell bacterial detection. *Clin Microbiol Rev* 27:631–646.
- Asally M, et al. (2012) Localized cell death focuses mechanical forces during 3D patterning in a biofilm. *Proc Natl Acad Sci USA* 109:18891–18896.
- Young JW, et al. (2011) Measuring single-cell gene expression dynamics in bacteria using fluorescence time-lapse microscopy. *Nat Protoc* 7:80–88.